

Spectral data treatments for impervious endmember derivation and fraction mapping from Landsat ETM+ imagery: a comparative analysis

Wei WANG¹, Xinfeng YAO², Minhe JI (✉)^{1,3}, Jiao ZHANG¹

¹ Key Laboratory of GIScience (Ministry of Education of China), East China Normal University, Shanghai 200241, China

² Agricultural Information Institute of Science and Technology, Shanghai Academy of Agricultural Sciences, Shanghai 201403, China

³ China East-West Cooperation Research Center, East China Normal University, Shanghai 200241, China

© Higher Education Press and Springer-Verlag Berlin Heidelberg 2014

Abstract Various spectral data preprocessing approaches have been used to improve endmember extraction for urban landscape decomposition, yet little is known of their comparative adequacy for impervious surface mapping. This study tested four commonly used spectral data treatment strategies for endmember derivation, including original spectra, image fusion via principal component analysis, spectral normalization, and the minimum noise fraction (MNF) transformation. Land cover endmembers derived using each strategy were used to build a linear spectral mixture analysis (LSMA) model in order to unmix treated image pixels into fraction maps, and an urban imperviousness map was generated by combining the fraction maps representing imperviousness endmembers. A cross-map comparative analysis was then performed to rank the four data treatment types based on such common evaluation indices as the coefficient of determination (R^2) and root mean square error (RMSE). A Landsat 7 ETM+ multispectral image covering the metropolitan region of Shanghai, China was used as the primary dataset, and the model results were evaluated using high-resolution color-infrared aerial photographs of roughly the same time period. The test results indicated that, with the highest R^2 (0.812) and the lowest RMSE (0.097) among all four preprocessing treatments, the endmembers in the form of MNF-transformed spectra produced the best model output for characterizing urban impervious surfaces. The outcome of this study may provide useful guidance for future impervious surface mapping using medium-resolution remote sensing data.

Keywords impervious surface estimation, linear spectral

mixture analysis, minimum noise fraction, spectral normalization, image fusion

1 Introduction

Impervious surfaces, generally defined as anthropogenic features that water cannot infiltrate, are commonly recognized as a key indicator in assessing the health of urban ecosystems and environmental quality (Arnold and Gibbons, 1996). Their estimation in urban areas has been increasingly relying on remote sensing, especially with medium spatial resolution imagery, which provides complete coverage for large areas with low costs (Ji and Jensen, 1999; Lu and Weng, 2006). On the other hand, medium-resolution imagery is prone to the so-called “mixed pixel” problem. This problem is defined as the spectral mixture of more than one material within a single pixel due to the high degree of heterogeneity of urban landscapes (Lu et al., 2011). The presence of mixed pixels may significantly degrade urban mapping quality and affect the effective use of remote sensing data for urban applications.

Among numerous methods that have been proposed to cope with mixed pixels (Ji and Jensen, 1999; Wu and Murray, 2003; Mohapatra and Wu, 2008; Hu and Weng, 2009; Im et al., 2012), linear spectral mixture analysis (LSMA) is most widely used with medium-resolution remote sensing data (Lu et al., 2003; Wu and Murray, 2003; Lu et al., 2004; Lu and Weng, 2004; Ji and Feng, 2011). LSMA is a physically based image processing method that assumes the per-pixel radiance to be a linear combination of the endmember spectra of all ground materials within the image scene. Theoretically, LSMA is capable of improving land cover classification accuracy by

modeling the spectral mixture of a pixel from adequately derived endmembers (Lu et al., 2003, 2004; Lu and Weng, 2004). In practice, however, LSMA still faces some technical challenges. The most critical issue is centralized on how to select appropriate endmembers to represent major land cover types in an image scene, especially in highly heterogeneous urban areas with large spectral variation. One solution to this problem is to build a scene-oriented spectra library to support multiple end-member spectral mixture analysis (MESMA) so that spectral constituents of each land cover type can be mapped into separate endmembers (Roberts et al., 1998; Rashed, 2008). In most applications, however, a simpler approach is adopted, i.e., preprocessing spectral data in favor of endmember selection through a chosen data treatment strategy.

Various data preparation techniques have been designed to make multispectral imagery more suitable for end-member detection. Principal component analysis (PCA) (Smith et al., 1985) and minimum noise fraction (MNF) transformation (Green et al., 1988) have been used to compress multispectral data with high between-band correlation into fewer uncorrelated components. With the majority of information distilled from the original spectra, these components are then used to construct a transformed space capable of delineating spectra of different land cover types more easily and accurately (Wu and Murray, 2003; Lu and Weng, 2004). An alternative data preparation method is spectral data normalization, as coined by Wu (2004). This method aims to reduce the brightness variation of image pixels within individual urban land cover components, e.g., vegetation, impervious surface, and soil, thus allowing a component to be represented by just one single endmember. Further studies have shown that component-oriented spectral normalization is an effective tool for identifying endmembers (Yuan and Bauer, 2007; Chen and Li, 2008; van de Voorde et al., 2009). Along with the recent growing interest in pan-sharpening of multispectral data for improved spatial resolution (Li et al., 2002; González-Audícana et al., 2005; Jing and Cheng, 2011; Ji et al., 2012; Yang et al., 2012), image fusion has also been used to reduce the complexity of mixed pixels by introducing spatial details through the readjustment of image intensity (Zurita-Milla et al., 2011). Further, the texture and context information derived from the panchromatic band helped to identify endmembers (Lu and Weng, 2005).

While the above data treatment routines have proven effective in their respective application settings, knowledge about their relative strength and weakness in dealing with the same spectral dataset obtained from a highly complex and heterogeneous urban area is still lacking in the literature. Practical guidance is needed regarding which data preparation approach is appropriate when remote sensing analysts are faced with multiple methodological choices. A comparison of different data treatment types on

endmember extraction would help to highlight the strengths and weaknesses of each approach for spectral data preprocessing. It may also reveal some influential factors to be considered for further improvement of mapping urban impervious surfaces. The objective of this paper, therefore, was to examine the effects of the aforementioned four types of spectral data treatments (i.e., original spectra with no treatment, MNF transformation, PCA-based image fusion, and spectral normalization) on urban impervious surface mapping.

In this empirical study, a Landsat ETM+ image covering the Central Business District (CBD) and its vicinity of Shanghai, China was employed as the primary test data, and some aerial photos within the study area were obtained for result verification. The remaining text is organized as follows. The next section introduces the study area and datasets, followed by the third section describing the methodological design and experimental procedure. A comparative analysis of the imperviousness maps resulting from different data treatment methods is presented in the fourth section. The last section concludes with a summary of the work and suggestions for future research.

2 Study area and data

The region under investigation covers the central portion of Shanghai, China (Fig. 1) with a total area of approximately 633 km². Located in the forefront of Yangtze River Delta (centered at 31°14'N and 121°29'E), the city of Shanghai enjoys its position as the second largest metropolitan region in China. Ever since 1978 when China's national economic reform started, Shanghai has been undergoing rapid urban growth in both population and area. A tremendous amount of agricultural lands have been turned over to residential, commercial, and industrial uses over the years, resulting in a huge increase and restructuring of impervious surfaces in the urbanized area. Accurate impervious surface information is crucial to urban planning and environmental management in Shanghai.

A cloud-free, high-quality Landsat 7 ETM+ image (path 118/row 38) of Shanghai, acquired on July 3, 2001, was used as the primary dataset in this study. Provided by the USGS Earth Resource Observation Systems Data Center, the image was preprocessed for radiometric and geometrical correction to the 1G quality level before delivery. This image was further projected onto the Universal Transverse Mercator coordinate system. In addition, a set of color-infrared aerial photographs, dated March and April of 2000, were acquired for validation. These digital aerial photographs possessed a 0.6-m spatial resolution and were spatially registered to the ETM+ data for further analysis (Fig. 1).

Due to the possibility of interference by water features on the extraction of low-reflectance impervious surfaces

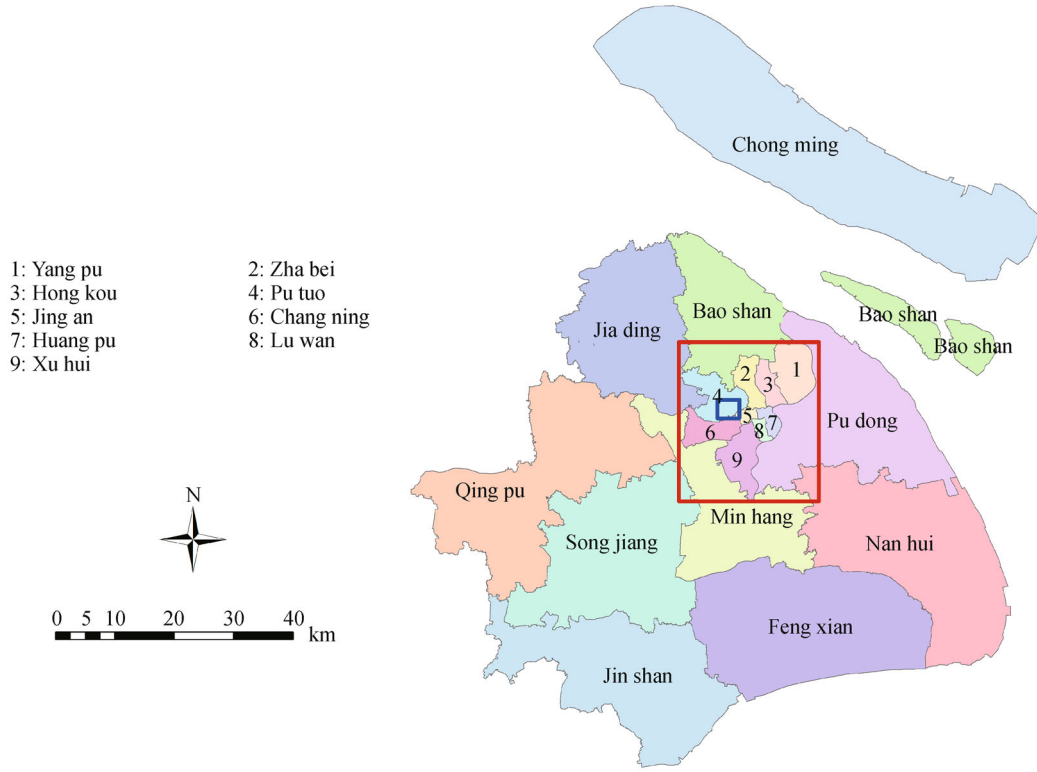


Fig. 1 Study area: Shanghai CBD and its vicinity (The red box delineates the main study area, and the blue box indicates the coverage of validation data).

during the spectral mixture analysis (Wu, 2004), water bodies such as lakes and rivers were removed from the ETM+ image via a mask generated from the modified normalized difference water index (MNDWI) (Xu, 2006) as expressed below:

$$\text{MNDWI} = (B5 - B2) / (B5 + B2), \quad (1)$$

where B2 and B5 are the red and first mid-infrared bands of the ETM+ multispectral image, respectively. The threshold value of MNDWI for the water mask was finally determined to be 0.05 through multiple trial-and-error experiments aided by visual inspection.

All image processing and result visualization were performed using ENVITM 5.0, and the linear spectral mixture analysis and post-estimation analysis were implemented in MATLABTM 2012a.

3 Methods

The term “data treatment” to be used in this study refers to the preparation of spectral data in a specific way. The treated spectra will be used to generate MNF-based scatter plots for endmember selection, and then used in the LSMA modeling and classification process. The procedure for the different spectral data treatment techniques compared in

this paper is shown in Fig. 2. In the case of original spectra with no treatment, for instance, the ETM+ pixel reflectance values will be transformed into an MNF component space for interactive endmember selection, and classified using the LSMA model built with the original spectra of selected endmembers. Likewise, any other data treatment approaches will not only engage an MNF transformation of the treated data for endmember selection but also use the transformed data as the basis for the subsequent LSMA modeling and classification. For the sake of comparison, it is instructive to provide more details about each of the data treatment techniques below.

3.1 Spectral normalization

Spectral normalization is applied to reduce the brightness variation of each V-I-S component. With increased within-class homogeneity, it is expected that subsequent image analysis may provide improved results (Wu, 2004). Spectral normalization is achieved by rescaling the pixel value in each band over the average value of all bands for the same pixel, formally expressed as

$$\bar{R}_b = \frac{R_b}{\mu} \times 100, \quad \mu = \frac{1}{N} \sum_{b=1}^N R_b, \quad (2)$$

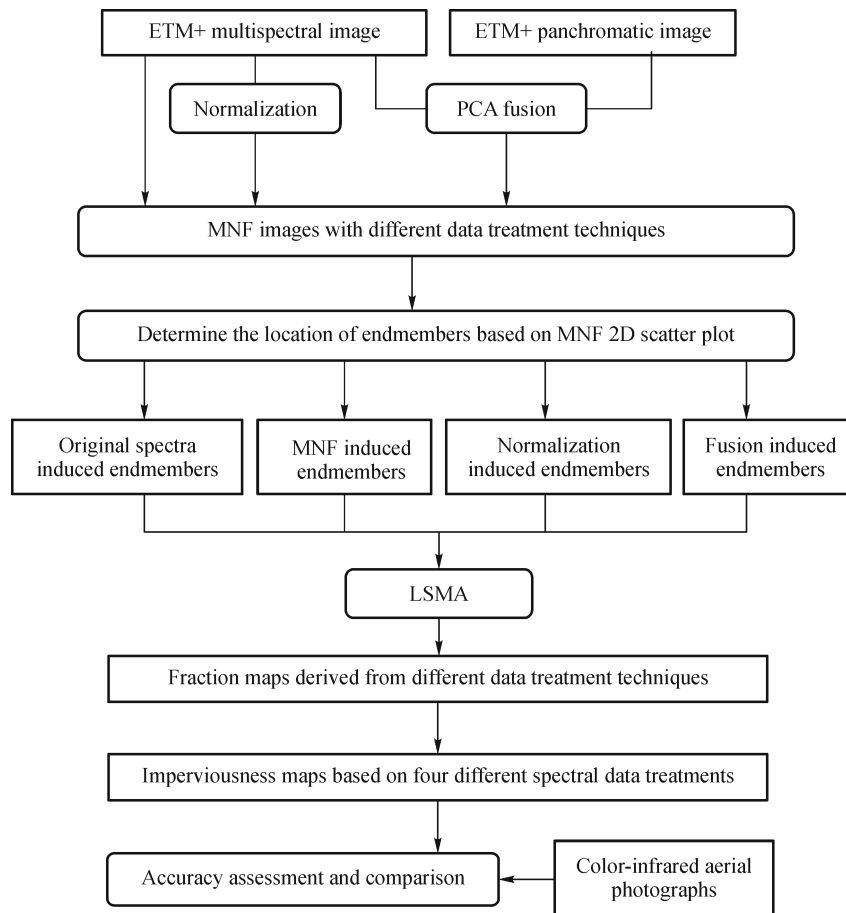


Fig. 2 Procedure for comparing the effects of different spectral data treatment techniques on impervious surface mapping.

where R_b is the original reflectance for band b in a pixel, \bar{R}_b is the normalized reflectance for band b , μ is the average reflectance in a pixel, N is the total number of spectral bands.

3.2 Image fusion

Image fusion is achieved via replacing the intensity component of the multispectral image with an image (usually panchromatic image) of higher spatial resolution (González-Audicana et al., 2004). Specific to the ETM+ data, image fusion can be used to incorporate rich textural information from the 15-m panchromatic band into the 30-m multispectral data for improved estimation of impervious surface areas (Lu et al., 2011).

Many image fusion methods exist, but principal component analysis (PCA) was chosen for this study because of its proven ability to preserve the spectral integrity of the input images (Lu and Weng, 2005). The PCA-based image fusion procedure consists of four steps: a) resample the spectral data of the ETM+ six bands to the resolution of the panchromatic image, b) transform resampled multispectral bands into six principal compo-

nents (PCs), c) replace PC1 (treated as the intensity component) with the panchromatic image, and d) reversely transform all six PCs back to the multispectral space (Chavez et al., 1991). The result of this procedure is a six-band image containing the spectral data most resembling the original ETM+ image but having a spatial resolution of 15 m.

3.3 Minimum noise fraction transform

The minimum noise fraction (MNF) method removes between-band collinearity through orthogonal transformation, using the first few components accounting for the majority of variance in the original image (Green et al., 1988). MNF is a common practice in LSMA-based imperviousness extraction, used to make endmembers more identifiable (Lu and Weng, 2004). The usual practice of MNF in LSMA applications is for endmember selection only, that is, the transformed data is only involved in the construction of an MNF space for pure pixel identification but not used in the later classification (Lu and Weng, 2004). As a comparing method, however, we hereby deliberately use the MNF scores of each endmember

directly to build an LSMA model for endmember fraction mapping.

3.4 Endmember selection

The endmember selection in each data treatment case follows the usual MNF-based procedure (Fig. 2). The MNF components are first generated from each of the four experimental datasets, and three 2-D scatterplots are then constructed by pairing the first three MNF components. The distributional pattern of plotted pixels is examined in the plot to visually locate pure pixels that can be used to represent individual endmembers. The typical pure pixels are those located at the extreme vertices of the data cloud in the scatterplots. Finally, the endmember spectra for each case are obtained from the respective preprocessed image by linking the pure pixel in the MNF space back to the image feature space. It is worth noting that both the original data and MNF transformed data produce a set of identical endmembers in the MNF space, but in the latter case, it is the transformed scores rather than the original spectra that are used to represent the endmembers in LSMA modeling. The end products of this procedure are four sets of endmembers, each representing one land cover type of interest in the targeted urban environment from a specific data treatment perspective. These endmember sets are used as model input for the subsequent LSMA modeling.

3.5 Linear spectral mixture analysis

The LSMA assumes that the reflected radiance of a pixel is a linear combination of the spectral endmembers representing major land cover types within the scene. Therefore, the LSMA model can be formally expressed as

$$R_{mj} = \sum_{i=1}^n f_{ij} R_{im} + \varepsilon_{mj}, \quad (3)$$

where $i = 1, \dots, n$, n is the number of endmembers; R_{mj} is the reflectance for band m in pixel j ; R_{im} is the spectral reflectance of band m of endmember i ; ε_{mj} is the error for band m and pixel j ; f_{ij} is the fraction of endmember i in pixel j . For a constrained unmixing solution, f_{ij} is subject to the following restrictions:

$$\begin{aligned} \sum_{i=1}^n f_{ij} &= 1 \\ f_{ij} &\geq 0. \end{aligned} \quad (4)$$

Due to the existence of high spectral heterogeneity among urban impervious materials, it is extremely difficult to give a singular definition to the endmember known as ‘‘imperviousness’’ (Wu and Murray, 2003; Lu and Weng, 2004). This issue has been coped with by spectrally

separating imperviousness into low and high albedo endmembers during the LSMA modeling (Wu and Murray, 2003; Wu, 2004). In this way, a constrained least squares solution is applied in this study in order to unmix the six bands of the ETM+ image into four fraction maps (i.e., vegetation, high-albedo imperviousness, low-albedo imperviousness, and soil). The final imperviousness map will be the combination of both high-albedo and low-albedo fraction maps.

3.6 Accuracy assessment and cross-map comparison

The accuracy of urban imperviousness derived from each of the four experimental datasets was assessed with the reference data manually interpreted from the color-infrared digital aerial photographs within the same study area. The resolution of the aerial photos was downscaled from 0.6 m to 9.0 m for the convenience of visual comparison. A total of 100 sample sites were randomly selected from the validation area. Each site was sampled with a 3×3 window, yielding a coverage of $90 \text{ m} \times 90 \text{ m}$ on the fraction maps and a corresponding 10×10 window on the aerial photographs. The intention of such a sampling design is to minimize the effect of image-to-image misregistration and make it relatively easy to compute the reference fraction for each sample site. The reference fraction was calculated from the aerial photographs as follows. First, each 9-m pixel within the sample site area was visually determined as being either impervious or pervious. Second, the impervious pixels were tallied and aggregated for the site. Third, the fraction was computed by dividing the number of impervious pixels by the total number of pixels within the site area (100 in this study). The averaged fraction from the corresponding nine pixels in the fraction map was used to compare with the reference fraction in the accuracy assessment.

The cross-map comparison was performed on the basis of two commonly used map accuracy indices, the coefficient of determination (R^2) and root mean square error (RMSE). The calculation of R^2 followed the standard statistical procedure, which is not further detailed here. A positive and significant high value of R^2 between predicted and observed values is considered to indicate that high-quality endmembers are being extracted from the treated dataset. The second accuracy indicator, RMSE, is defined as

$$\text{RMSE} = \sqrt{\frac{\sum_{i=1}^n (ISE_i - ISO_i)^2}{n}}, \quad (5)$$

where ISE_i is the estimated impervious surface fraction for sample i , ISO_i represents the impervious surfaces proportion observed from the reference data for sample i , and n is the number of samples. In this case, low RMSE values indicate a good fit between predicted impervious surfaces

and the reference data. In addition, the scatterplots of the 1:1 relationship between observed and predicted values were generated for further examination of model errors (Wu and Murray, 2003).

4 Experimental results and discussion

4.1 Endmembers and their characteristics

Due to the high level of spectral complexity in the Landsat ETM+ image of urban Shanghai, we expanded the generic V-I-S model into a vegetation-high albedo-low albedo-soil (V-H-L-S) model, which was represented by four endmembers, i.e., vegetation, high-albedo, low-albedo, and soil. Imperviousness was hereby comprised of high-albedo and low-albedo to cope with the spectral diversity of the

urban land cover type in the study area. Each treated dataset was transformed into MNF space and visualized in the MNF 2D scatterplots for endmember selection. The identified endmembers were graphed as characteristic curves for each treatment type (Fig. 3).

It is rather interesting to see from these spectral curves (Fig. 3) that all treatment types except MNF share a highly similar reflectance pattern for vegetation, and less so for the other three endmembers. This is because MNF has transformed the original spectra into an entirely different feature space. On the other hand, MNF seems to have enlarged the gaps between different endmembers in the first three components, leading to a higher overall separability in its subsequent LSMA modeling. In addition, the application of spectral normalization effectively reduced the spectral diversity among all endmembers, and even made soil, high-albedo, and low-albedo fit into the same data range.

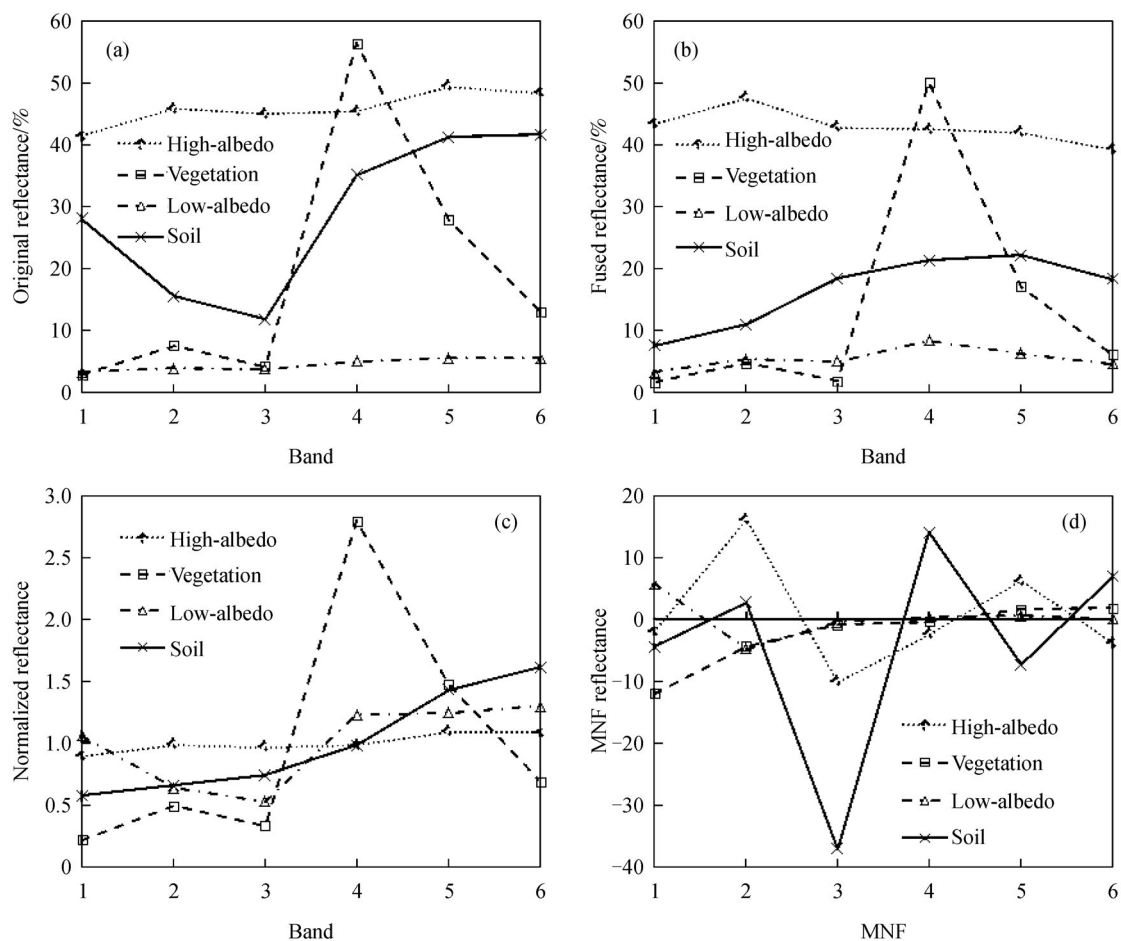


Fig. 3 Reflectance (original or transformed) characteristics of endmembers for the four data treatment types: (a) original spectra, (b) fused spectra, (c) normalized spectra, and (d) MNF spectra.

4.2 Generation of fraction maps for endmembers and imperviousness

The fraction map for each urban endmember was obtained by solving the fully constrained linear spectral mixture model given in Eq. (3). A total of 16 fraction maps were generated and grouped into four sets, with each row corresponding to one type of data treatment (Fig. 4). Visual inspection revealed that maps of the same endmember shared a similar spatial distribution pattern across all treatment types. For instance, high values of high-albedo and low-albedo imperviousness tend to concentrate in the central region of the study area, and the fraction values for vegetation increase with distance from the CBD. Since the study area was heavily urbanized, the soil endmember exhibited relatively low fraction values all over the map in all four cases.

Despite the similarity in distributional patterns, major differences also existed among treatment types for the same endmember, especially with respect to fraction levels. Maps resulting from the original spectra and the MNF treatment look highly similar (maps on row 1 and row 2 in Fig. 4), except that vegetation seems better characterized in the MNF case. This is especially evident when a forest park located at the upper-right corner of the map is examined. It suggested that the MNF transformation was capable of enhancing the spectral distinction of endmembers by removing data collinearity and noise. In comparison, image fusion seemed to produce a great number of high fractions in high albedo and soil by lowering the abundance of vegetation and low albedo (maps on row 3 in Fig. 4). This might be caused by the side-effect of introducing spatial details during the fusion process, i.e., increasing the spectral contrast by splitting the mixed pixels located in urban residential areas. The fraction maps of normalized spectra are also very revealing (maps on row 4 in Fig. 4). This treatment seemed to provide a fair definition of low-albedo imperviousness, as the urban transportation lines, usually paved by asphalt, a material type typically with low spectral reflectance in all bands, were clearly highlighted in the scene. Likewise, vegetation was more clearly delineated and had greater fraction values compared to other treatment types. This demonstrated the spectral purification effect of the method, i.e., homogenizing the spectra of mixed pixels toward the dominating endmember, so as to sharpen the edges between features with high reflectance values and those with low values.

Four imperviousness maps (Fig. 5), each for a data treatment type, were generated by additively combining corresponding low-albedo and high-albedo fraction maps of the same treatment type. As expected from a good mapping result, these maps correctly show the concentration of high values in the CBD area and on the transportation corridors, giving a seemingly well characterized urbanization pattern in Shanghai.

4.3 Cross-treatment comparison of imperviousness fraction maps

Two comparative analyses were performed on the imperviousness fraction maps across data treatment types. The first comparison was aimed at understanding the relative behavior of different treatment types in impervious surface mapping. This was achieved by pairing the imperviousness fraction maps and calculating a difference map for each pair. This operation led to six difference maps' being generated. Based on the data treatment types involved in the operation, these difference maps were labeled as Fused-Original, Original-Normalized, Original-MNF, Fused-Normalized, Fused-MNF, and MNF-Normalized, respectively (Fig. 6). For the convenience of cross-map comparison, the fraction map of the image fusion treatment was resampled to 30 m.

Among all six difference maps in Fig. 6, Original-MNF exhibits a somewhat uniform pattern with the least variation over the entire study area, suggesting that using MNF-treated data for LSMA modeling tended to generate results very similar to those of using the original ETM+ data. The second least variation pattern appeared on MNF-Normalized, as most of its values were confined to ± 0.4 . In this map, the negative values are mostly associated with heavily impervious objects (e.g., buildings and roads), while the positive values are related to vegetated areas (e.g., parks and greenbelts), implying that the MNF treatment tended to produce a smaller value range for imperviousness fractions than the spectral normalization method. The positive values in the high end revealed the tendency of normalized spectra to regard vegetation-dominated urban areas as being completely pervious, as evident in the forest park located at the upper-right corner of the map. Similar patterns also appear in the Original-Normalized map, and even more imperviousness defined by the original spectra was inverted to pervious surfaces by spectral normalization.

On the other hand, Fused-MNF and Fused-Original share the same fraction difference pattern, and both have large fraction differences in the low end, indicating the tendency of image fusion to underestimate impervious features with saturated spectral values. Due to the enhanced image intensity, fused spectral data seemed to have uplifted the fraction level of some built objects (e.g., airport runways and building roofs made of special materials). Interestingly, the Fused-Normalized map integrates the above two patterns, which reveal the opposite effects of these two data treatment methods on remote sensing data. Compared to normalized spectra, impervious fractions produced using fused data tended to be over-emphasized in regions with low levels of imperviousness and underrepresented in the high-level areas, thus making these two fraction maps the most dissimilar among all six pairs.

In order to complement the qualitative evaluation from

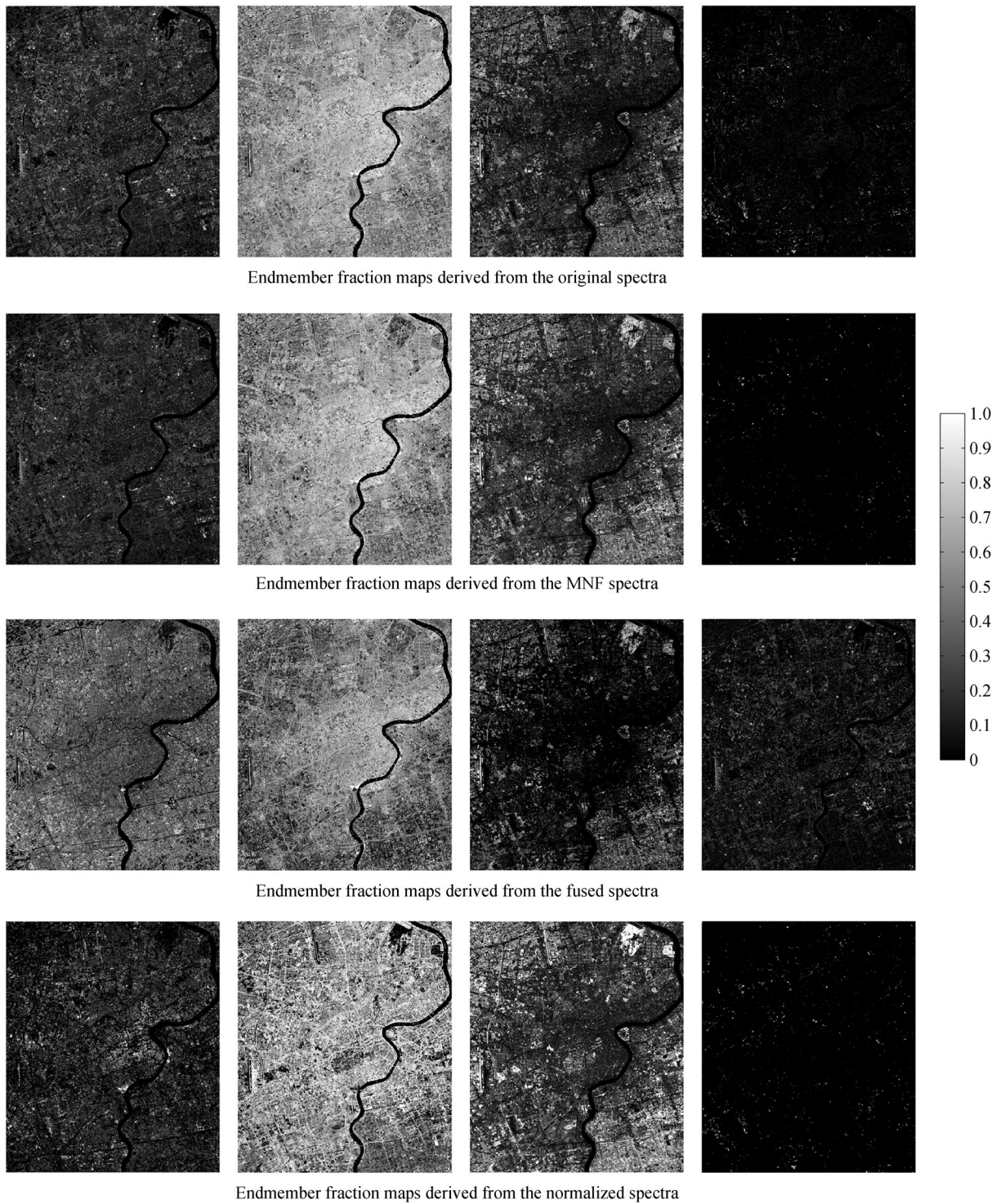


Fig. 4 Fraction maps resulting from the four data treatment types (columns from left to right: high albedo imperviousness, low albedo imperviousness, vegetation, and soil).

the above visual comparisons, a quantitative map accuracy assessment was then performed against reference data. Following the map assessment procedure proposed in

Section 3.6, R^2 and RMSE were computed from the 100 sampled points for each data treatment method and documented in Table 1. Among all treatment strategies,

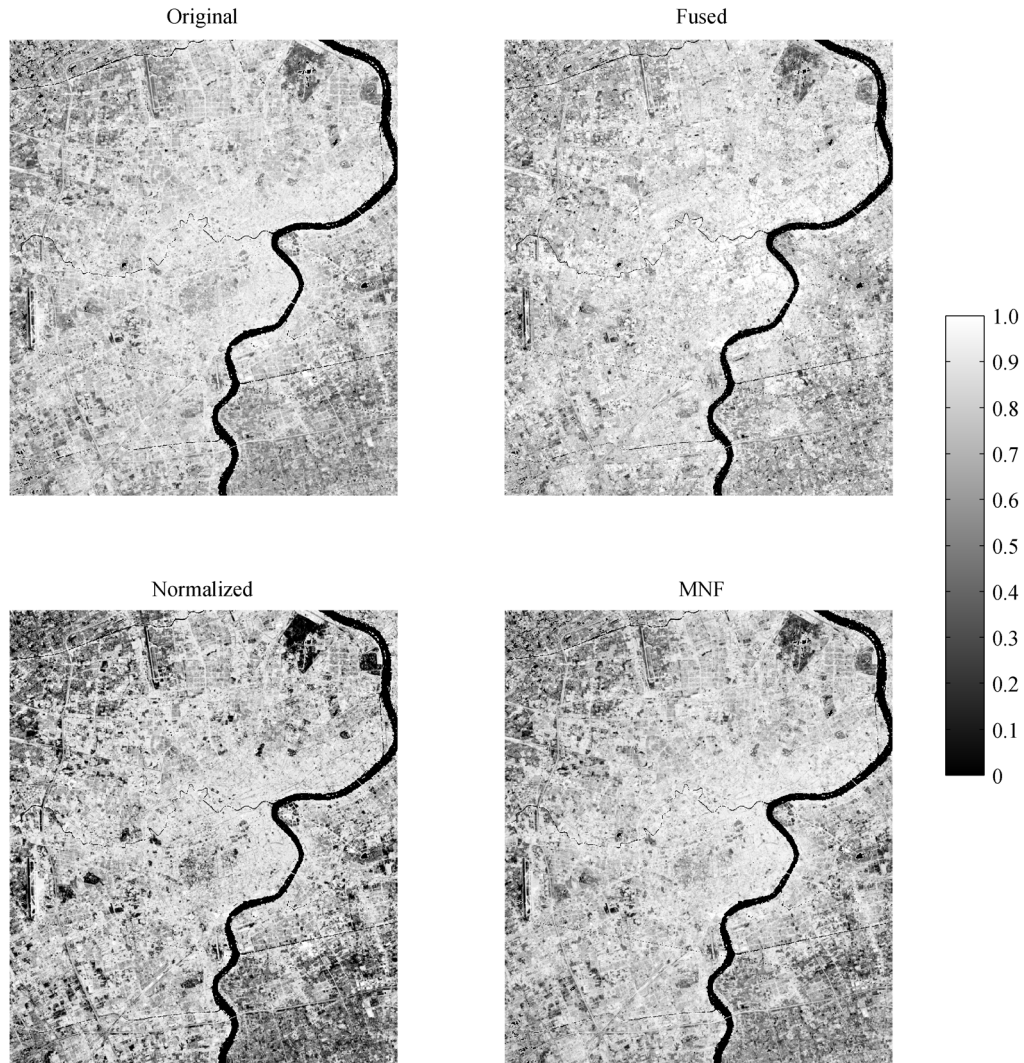


Fig. 5 Urban imperviousness maps resulting from the four data treatment types.

MNF produced the best result, whereas the fused image presented the worst case. Estimation using the original spectra produced a result highly similar to that of MNF. While plausibly conforming to the distribution pattern of imperviousness in Shanghai in the previous visual analysis, spectral normalization did not produce satisfactory results. The scatterplots of sampled points and the regression fitting lines in Fig. 7 provide some visual cues about the correlation strength between estimated fractions and reference data for the four data treatment approaches. It is rather apparent that the values of sample points are relatively dispersed in the fused and normalized cases and tightly converged in the MNF and the original spectra cases.

4.4 Further discussion

The assessment of the fraction maps presented above

provides useful insights into the four spectral data treatment strategies being compared in this study. The original spectra apparently contain full and undistorted information from the urban environment, so they provide the best possible potential for characterizing any end-member of interest. However, due to the high collinearity among the spectral bands, this potential may not be fully realized with respect to an urban endmember with complex and diverse spectral characteristics. In comparison, the MNF scores transformed from the original spectra seem less plagued by the spectral overlapping problem, as the method is theoretically able to rotate the axes of the original spectra to a new set of mutually orthogonal positions. As a result, data treated with MNF performed better than the original spectra in this case study. This observation was also confirmed in other relevant studies (Wu and Murray, 2003; Lu and Weng, 2004; Wu, 2009).

The results from image fusion did not meet the initial

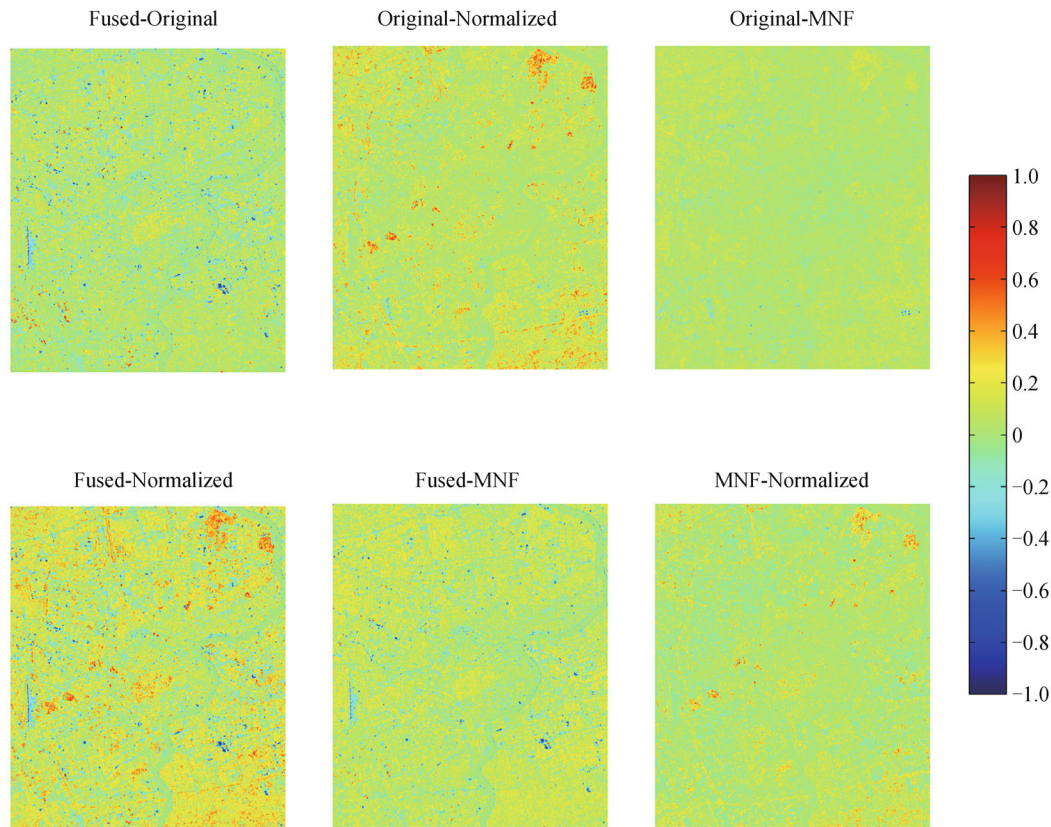


Fig. 6 Cross-treatment comparison of imperviousness fraction maps.

Table 1 Accuracy measures of impervious surface fraction maps induced from different spectra: original, fused, normalized, and MNF

Error	Original LSMA	Fused LSMA	Normalized LSMA	MNF LSMA
R^2	0.7952	0.5185	0.7642	0.8120
RMSE	0.0972	0.1465	0.1417	0.0965

expectation of this study. The low level of accuracy might have been caused by the altered spectral characteristics of impervious pixels when a great number of textural details are introduced. Instead of reducing the amount of mixed pixels in the scene, the treatment seemed to have complicated the problem by enlarging the spectral variance of each endmember (Lu and Weng, 2005). Consequently, even the purest training sites might have been contaminated by the insertion of spatial details, making it less representative of a given cover type (Wu, 2009). This was evident among the third-row fraction images in Fig. 4, where the inter-endmember confusion drastically increased between high and low albedos, as well as low albedo and soil. Compared to the other data treatment approaches, the impervious surface induced from the fused spectra contained some outliers in several isolated locations (Fig. 6), very likely attributable to severe distortion of the original spectra during the fusion process. Overall, this

implies that image fusion at medium resolution may not be a good choice for an urban area with high structural complexity and spatial heterogeneity.

The initial intention of using spectral normalization was to suppress data anomalies so that the spectral heterogeneity of each endmember could be reduced (Wu, 2004). Results from this study have clearly demonstrated the existence of such an effect, but it led to degradation, rather than improvement, of imperviousness modeling. In contrast to image fusion, spectral normalization works in an opposite way, homogenizing data in favor of the spectra of the dominating ground cover types in the pixel. As a result, areas dominated by pervious features (e.g., forests or parks) tend to be overestimated as being completely pervious. This issue was also observed by Yuan and Bauer (2007) and discussed in other studies (Chen and Li, 2008; van de Voorde et al., 2009). Given the spectral complexity of urban impervious surfaces, using a simple spectral

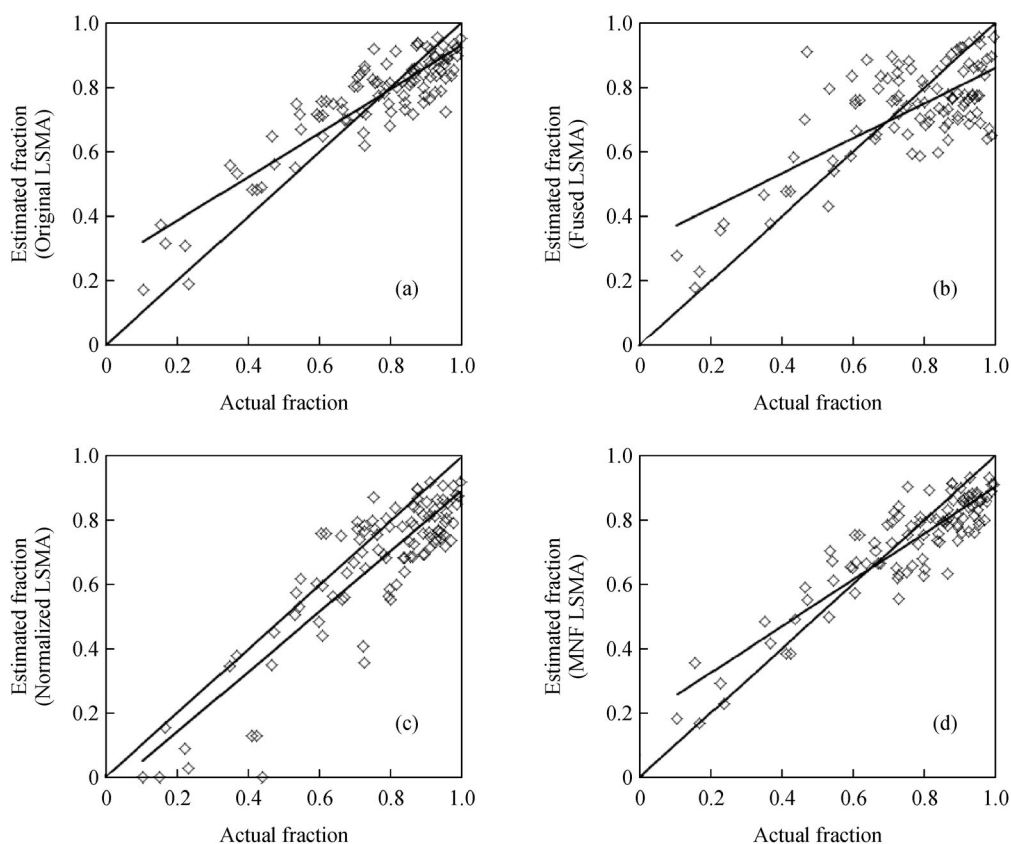


Fig. 7 Scatterplots and regression lines of accuracy validation sample points for each type of data treatment: (a) original, (b) fused, (c) normalized, and (d) MNF.

normalization may not be an adequate solution. Although there was no test in this study to evaluate endmembers other than imperviousness, caution must be taken when choosing spectral normalization for endmember selection.

5 Conclusions

This study compared the performances of four different spectral data treatment routines for impervious surface estimation via LSMA from Landsat ETM+ multispectral imagery. For each treatment method, fraction maps of four endmembers (i.e., vegetation, high-albedo, low-albedo, and soil) representing the urban landscape of Shanghai were generated and analyzed. The impervious surface fraction maps resulting from different treatments were statistically validated and compared. Among all, the MNF transformation exhibited the best performance in imperviousness estimation, followed by the original spectra with no treatment. Data processed by spectral normalization and image fusion did not produce good results. Due to the nature of their respective processing mechanisms, the former tended to overestimate imperviousness located in

the low end of the fraction scale, whereas the latter are inclined to underestimate imperviousness in pixels dominated by pervious spectra.

Although the MNF approach has been ranked the best for impervious surface mapping in this study, the achieved accuracy level (i.e., 0.81) is still considered unsatisfactory by the de facto standard of 0.85, a magic figure widely accepted in the remote sensing community (Foody, 2002). This situation implies that the urban imperviousness in Shanghai is even more complex than what was conceptualized and so modeled in this LSMA layout. It might require either a further breakdown of imperviousness rather than just high and low albedos or more thorough removal of water spectra from the original image. In the former case, for instance, low albedo needs a finer definition so that it can become more distinctive from the vegetation spectra (see Fig. 3(d) for their confusion). Methods of nonlinear spectral unmixing (Hu and Weng, 2009; Im et al., 2012) and multiple endmember spectral mixture analysis (Lu and Weng, 2004; Powell et al., 2007) may be good options to use for tackling this problem. The latter case is related to the confusion of low-albedo with water. The fact that widespread water pollution and

numerous subpixel-level water bodies exist in Shanghai made the removal of them extremely difficult. Solutions to this issue may need to be developed using such ancillary data as large-scale GIS hydrography layers and low-altitude aerial photographs through visual interpretation.

Acknowledgements This work was supported by the National Basic Research Program of China (No. 2010CB951603). Our gratitude goes to Prof. Jianhua Zhou for her generous sharing of the historical color-infrared aerial photographs to be used for accuracy assessment in this project. We also thank the International Scientific Data Service Platform, Computer Network Information Center, and the Chinese Academy of Sciences for providing the Landsat 7 Enhanced Thematic Mapper Plus image data.

References

- Arnold C L Jr, Gibbons C J (1996). Impervious surface coverage: the emergence of a key environmental indicator. *J Am Plann Assoc*, 62(2): 243–258
- Chavez P S, Sides S C, Anderson J A (1991). Comparison of three different methods to merge multiresolution and multispectral data—Landsat TM and SPOT panchromatic. *Photogramm Eng Remote Sensing*, 57(3): 295–303
- Chen X, Li L (2008). A comparison of spectral mixture analysis methods for urban landscape using Landsat ETM+ data: Los Angeles, CA. *Proceedings of the International Archives of the Photogrammetry, Remote Sensing and Spatial Information Sciences*. Beijing, China: 635–640
- Foody G M (2002). Status of land cover classification accuracy assessment. *Remote Sens Environ*, 80(1): 185–201
- González-Audícana M, Otazu X, Fors O, Seco A (2005). Comparison between Mallat's and the 'à trous' discrete wavelet transform based algorithms for the fusion of multispectral and panchromatic images. *Int J Remote Sens*, 26(3): 595–614
- González-Audícana M, Saleta J L, Catalán R G, García R (2004). Fusion of multispectral and panchromatic images using improved IHS and PCA mergers based on wavelet decomposition. *IEEE Transactions on Geoscience and Remote Sensing*, 42(6): 1291–1299
- Green A A, Berman M, Switzer P, Craig M D (1988). A transformation for ordering multispectral data in terms of image quality with implications for noise removal. *IEEE Transactions on Geoscience and Remote Sensing*, 26(1): 65–74
- Hu X, Weng Q (2009). Estimating impervious surfaces from medium spatial resolution imagery using the self-organizing map and multi-layer perceptron neural networks. *Remote Sens Environ*, 113(10): 2089–2102
- Im J, Lu Z, Rhee J, Quackenbush L J (2012). Impervious surface quantification using a synthesis of artificial immune networks and decision/regression trees from multi-sensor data. *Remote Sens Environ*, 117: 102–113
- Ji M, Chen W, Wang W (2012). Improving spectral fidelity of WorldView-2 image fusion via a constrained generalized intensity-hue-saturation model with localized weight structure through land cover classification. *J Appl Remote Sens*, 6(1): 061707
- Ji M, Feng J (2011). Subpixel measurement of mangrove canopy closure via spectral mixture analysis. *Front Earth Sci*, 5(2): 130–137
- Ji M, Jensen J R (1999). Effectiveness of subpixel analysis in detecting and quantifying urban imperviousness from Landsat Thematic Mapper imagery. *Geocarto Int*, 14(4): 33–41
- Jing L, Cheng Q (2011). An image fusion method for misaligned panchromatic and multispectral data. *Int J Remote Sens*, 32(4): 1125–1137
- Li S, Kwok J T, Wang Y (2002). Using the discrete wavelet frame transform to merge Landsat TM and SPOT panchromatic images. *Inf Fusion*, 3(1): 17–23
- Lu D, Batistella M, Moran E, Mausel P (2004). Application of spectral mixture analysis to Amazonian land-use and land-cover classification. *Int J Remote Sens*, 25(23): 5345–5358
- Lu D, Hetrick S, Moran E (2011). Impervious surface mapping with Quickbird imagery. *Int J Remote Sens*, 32(9): 2519–2533
- Lu D, Moran E, Batistella M (2003). Linear mixture model applied to Amazonian vegetation classification. *Remote Sens Environ*, 87(4): 456–469
- Lu D, Weng Q (2004). Spectral mixture analysis of the urban landscape in Indianapolis with Landsat ETM+ imagery. *Photogramm Eng Remote Sensing*, 70(9): 1053–1062
- Lu D, Weng Q (2005). Urban classification using full spectral information of Landsat ETM+ imagery in Marion County, Indiana. *Photogramm Eng Remote Sensing*, 71(11): 1275–1284
- Lu D, Weng Q (2006). Use of impervious surface in urban land-use classification. *Remote Sens Environ*, 102(1–2): 146–160
- Mohapatra R P, Wu C (2008). Subpixel imperviousness estimation with IKONOS imagery: an artificial neural network approach. London: Taylor & Francis Group
- Powell R L, Roberts D A, Dennison P E, Hess L L (2007). Sub-pixel mapping of urban land cover using multiple endmember spectral mixture analysis: Manaus, Brazil. *Remote Sens Environ*, 106(2): 253–267
- Rashed T (2008). Remote sensing of within-class change in urban neighborhood structures. *Comput Environ Urban Syst*, 32(5): 343–354
- Roberts D, Gardner M, Church R, Ustin S, Scheer G, Green R (1998). Mapping chaparral in the Santa Monica Mountains using multiple endmember spectral mixture models. *Remote Sens Environ*, 65(3): 267–279
- Smith M O, Johnson P E, Adams J B (1985). Quantitative determination of mineral types and abundances from reflectance spectra using principal components analysis. *J Geophys Res*, 90(S02): C797–C804
- van de Voorde T, de Roeck T, Canters F (2009). A comparison of two spectral mixture modelling approaches for impervious surface mapping in urban areas. *Int J Remote Sens*, 30(18): 4785–4806
- Wu C (2004). Normalized spectral mixture analysis for monitoring urban composition using ETM+ imagery. *Remote Sens Environ*, 93(4): 480–492
- Wu C (2009). Quantifying high-resolution impervious surfaces using spectral mixture analysis. *Int J Remote Sens*, 30(11): 2915–2932
- Wu C, Murray A T (2003). Estimating impervious surface distribution by spectral mixture analysis. *Remote Sens Environ*, 84(4): 493–505
- Xu H (2006). Modification of normalised difference water index (NDWI) to enhance open water features in remotely sensed imagery.

- Int J Remote Sens, 27(14): 3025–3033
- Yang B, Kim M, Madden M (2012). Assessing optimal image fusion methods for very high spatial resolution satellite images to support coastal monitoring. *GIScience & Remote Sensing*, 49(5): 687–710
- Yuan F, Bauer M E (2007). Comparison of impervious surface area and normalized difference vegetation index as indicators of surface urban heat island effects in Landsat imagery. *Remote Sens Environ*, 106(3): 375–386
- Zurita-Milla R, Clevers J, Van Gijsel J, Schaepman M (2011). Using MERIS fused images for land-cover mapping and vegetation status assessment in heterogeneous landscapes. *Int J Remote Sens*, 32(4): 973–991